

# FLOW SIMULATION OF AN SST CONFIGURATION AT LOW-SPEED AND HIGH-LIFT CONDITIONS

Zhong Lei, Dong-Youn Kwak

Supersonic Transport Team, Japan Aerospace Exploration Agency  
7-44-1 Jindaiji-higashi, Chofu, Tokyo 182-8522, Japan

**Keywords:** *supersonic transport, high-lift device, vortical flow, aerodynamic performance*

## Abstract

*Flow field around a configuration of supersonic transport with high-lift devices at low speed and high angle of attack was investigated by solving Reynolds-averaged Navier-Stokes equations. The configuration was consisted of a fuselage and a cranked arrow wing, with deflected leading-edge and trailing-edge flaps. Numerical Simulations were conducted and validated at conditions of the wind-tunnel test. Details of flow field at the design condition were analyzed using computational results. Effect of the high-lift devices on aerodynamic performance was discussed. The leading-edge vortices were reduced both in size and in strength by deflecting the leading-edge flap and the drag was reduced. The trailing-edge flap increased the effective camber of the wing and improved the lift force. A typical leading-edge vortex flap was found. It was shown that the aerodynamic performance could be improved by deflecting the leading-edge and trailing-edge flaps.*

## 1 Introduction

Typical supersonic transports use low aspect ratio and highly swept wings to reduce wave drag at supersonic cruise conditions. However, a wing with large sweep angle of the leading edge is known for having poor aerodynamic efficiency lift-to-drag ratio for takeoff and landing at low speeds and high angles of attack. In order to meet economic viability and environmental compatibility, the next generation supersonic transport (SST) is required to have sufficient low speed performance in takeoff and landing situations. For example, Concorde generated

additional lift by encouraging vortices separated from its highly-swept leading-edge, and the additional vortex lift allowed Concorde to meet its takeoff and landing requirements. However, the leading-edge separation vortices reduced the effective lifting span and dramatically increased the induced drag. The additional thrust required to overcome the increased drag and the low speed performance deficiencies, generates an unacceptable engine noise and large fuel consumption.

To improve aerodynamic performance of the next generation SST at takeoff and landing situations, a high-lift system is desirable to enhance the lift as well as the lift-to-drag ratio [1][3][2]. Increased aerodynamic performance can reduce engine power setting and therefore community noise. One approach to improve the high-lift performance of a highly-swept wing at subsonic conditions is the use of a leading-edge vortex flap [4]. A suitable vortex flap locates the leading-edge vortex system on the forward facing area of a deflected flap, thus creates a low pressure region on the flap surface and results in a net thrust component. The trailing-edge flap can be used to increase the effective camber of the wing and therefore the lift.

Wind tunnel test plays an important role in the design process of an aircraft. On the other hand, numerical simulation of high-lift flows by solving the Reynolds-averaged Navier-Stokes (RANS) equations is now often used in analysis and design of high-lift devices. It can provide details of flow structure and help designer to understand the physics of high lift flow. Accurate predictions of aerodynamic characteristics are required for the design of the high-lift system. The objective of this study is to investigate

effect of high-lift devices on aerodynamic performance of an SST configuration, which consists of a cylindrical body and a cranked arrow wing (Fig. 1), and give insight into details of flow field at low speed and high angle of attack (AoA). Numerical simulation is conducted to solve the compressible Reynolds-averaged Navier-Stokes equations (RANS) with turbulence model and compared with experiment.

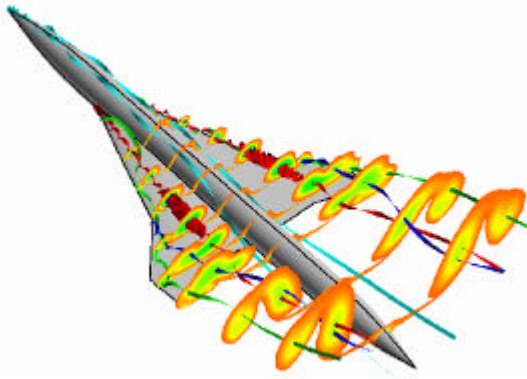


Fig. 1 Vortical flow around the SST configuration.

## 2 High-lift System

The computational model shown in Fig. 2 was a wing-body configuration of the so-called Jet01st baseline, which was designed preliminarily for a supersonic experimental airplane in Institute of Space Technology and Aeronautics of Japan Aerospace Exploration Agency (JAXA) [5]. The baseline model consisted of an axisymmetric body and a cranked arrow wing. The nose of the body was an ogive cone and the circular cylinder has a diameter 0.1m. The leading edge was kinked at 55% semi-span station of the wing. The inboard wing was designed as a subsonic leading edge with a sweep angle  $66^\circ$  to reduce the wave drag at the design Mach number of two and a NACA66 digit series with 3~6% maximum thickness was adopted as the thickness distribution. The leading-edge of the outboard wing was swept back by an angle  $42^\circ$  to increase the aspect ratio and improve the low-speed performance. The aspect ratio (AR) of the wing was 2.42. Finally, the wing was warped by Carlson's method to re-

duce lift-induced-drag at supersonic cruise conditions.

The inboard and outboard leading-edge flaps are shaded and deflected in takeoff and landing situations. The chord lengths of the leading-edge flaps are 10% mean aerodynamic chord (MAC) for the inboard wing and 20% local chord of the outboard wing from the leading-edge. The leading-edge flap deflections were obtained by rotating the flap along the hinge line to the desired deflection angle. In this paper, for the sake of simplification, names of configurations are represented by a numbering system,  $S_{xx}y_{yy}z_{zz}$ . Here, the indexes “xx”, “yy” and “zz” represent deflection angles of the inboard, outboard leading-edge and trailing-edge flaps, respectively. For example, S301210 means that the inboard, outboard leading-edge and trailing-edge flaps are deflected by  $30^\circ$ ,  $12^\circ$  and  $10^\circ$ . In this study, except the baseline S000000 model, several sets of inboard, outboard leading-edges and trailing-edge flaps are simulated. Flow field and aerodynamic characteristics are discussed.

Experiments were carried out by Kwak, et al [6] in a low speed wind tunnel of JAXA. Wind tunnel tests were ranged in  $-4^\circ \leq \alpha \leq +30^\circ$  angles of attack (AoA) at the air speed of freestream  $U = 30\text{m/sec}$  and Reynolds number  $0.945 \times 10^6$  based on MAC. Force and moment data were measured with an internal six-component balance system; surface pressure on the wing were measured at two chordwise stations, i.e.,  $X=0.55C_r$ ,  $0.83C_r$ .

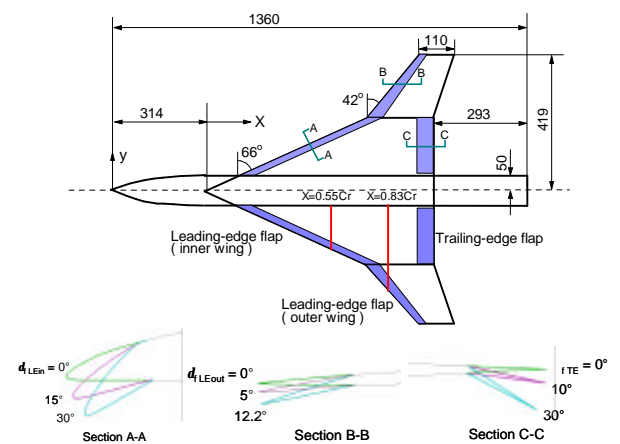


Fig. 2 The model of SST high-lift configuration.

### 3 Numerical Simulation

In numerical simulation, the freestream Mach number was set  $M=0.088$  to match the experiment conditions. An in-house flow solver, AeroDynamic Computational System (ADCS), was used to simulate the flow field and estimate the aerodynamic performance. The compressible Reynolds-averaged Navier-Stokes (RANS) equations are discretized using a finite difference method with multi-block technique. To simulate effect of turbulence, Menter's shear stress transport model was used. It has been validated for the computation of the vortical flow over the baseline configuration [7]. It uses the third-order TVD of Chakravarthy-Osher scheme for convection terms, central difference for other terms, and a diagonalized implicit method LU-ADI for time integration. At the entrance boundary, the total pressure, total temperature and the direction of incoming flow were specified to match the experimental conditions, while the velocity magnitude was obtained from the interior field by extrapolation. At the exit boundary velocities and density were extrapolated from interior field, only the static pressure was specified to be the reference value of the free-stream. On the solid surface, the no-slip condition was applied to the velocities and the normal derivative of pressure was forced to be zero. A symmetrical boundary condition is applied to the central plane.

In computation, an ogive cone tail was added to the body of the wind-tunnel model. H-H topology grid systems were generated around a half model of the configuration with a 5m width and 5m height. Grids were extended to 3m both upstream to the nose and downstream to the body tail. Grid points were carefully distributed in the normal direction of the surface to resolve the vortex structure. The spatial grid near the surface was forced normal to the configuration surface and the normal spacing of the first point from the surface was set to be  $1.0 \times 10^{-5}$  MAC. As an example, computational mesh around the high-lift configuration including the leading-edge and trailing-edge flaps, as shown in Fig. 3, contains about 7.2 million grid points.

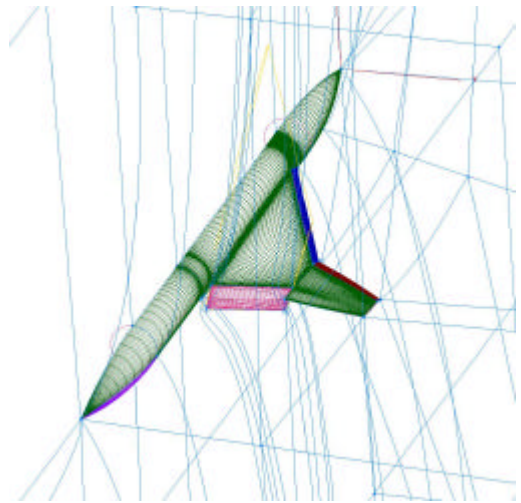


Fig. 3 Computational grids around the SST configuration.

### 4 Results and Discussions

Computational results for high-lift configurations will be given and compared with experimental data. Four models with different set of the leading-edge and trailing-edge flaps were simulated and analyzed. The baseline S000000 model does not have high-lift device; the S000010 model has a trailing-edge flap, which deflected down by  $10^\circ$ ; the S301200 model is a configuration with inboard and outboard leading-edge flaps deflected by  $30^\circ$  and  $12^\circ$ , respectively; the S301210 model has leading-edge flap deflected by  $30^\circ/12^\circ$ , and the trailing-edge flap deflected down by  $10^\circ$ . Effect of the leading-edge and trailing-edge flaps on the aerodynamic performance is discussed. Details of flow structure are analyzed using computational results to understand the mechanism of improvement of aerodynamic performance. The range of lift coefficient of interesting is from 0.4 to 0.8 for an SST at low speed region. Discussions will be focused on the cases of the AoA  $12^\circ$ , which is of interest in the design at takeoff and landing situations.

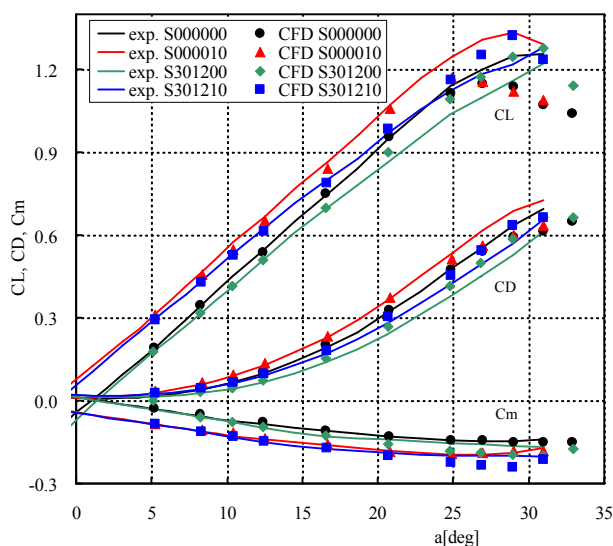
#### 4.1 Aerodynamic Performance

Aerodynamic characteristics of the four models are shown in Fig. 4. Experiment shows a de-

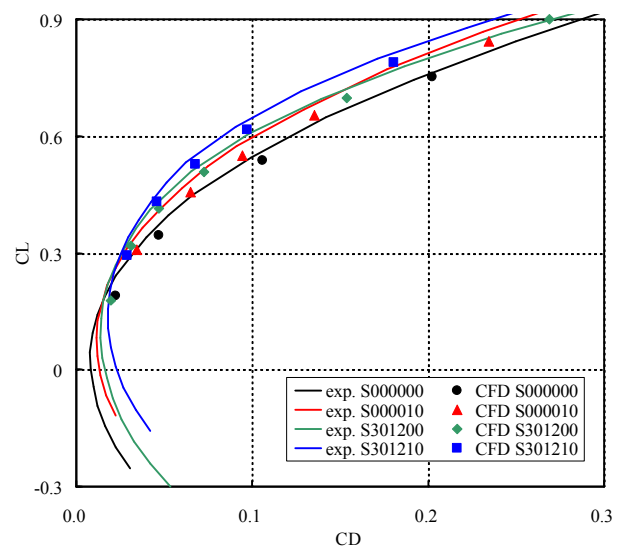
pendency on the deflection angle of the leading-edge and trailing-edge flaps. Effect of flaps on the aerodynamic forces is well reproduced by numerical simulation. Discrepancies between computation and experiment are observed because of the added body tail, assumption of fully turbulent flow and numerical error in computation. Computation is agreed well with experiment up to the AoA  $20^\circ$ , while the discrepancies become larger at high angles of attack. Small stall angles are predicted for all configurations due to the earlier vortex breakdown in computation.

By deflecting the leading-edge flap, the leading-edge vortices are suppressed and the additional lift due to vortex is reduced, so the lift and the lift- $\alpha$  slopes of the S301200 and S301210 models are smaller than those of the S000000 and S000010 models, respectively. The stall angle is also delayed. At lower angles of attack, the leading-edge separation is small and contributions little to the total aerodynamics forces. Because the leading-edge vortices increase the size and strength with increase of the angle of attack, deflection of the leading-edge

flap is more effective at moderate angles of attack. Generally, the drag is changed more rapidly with the strength of vortex than the lift does, so drag reduction is larger than the reduction of the vortex lift. As a result, the aerodynamic efficiency, i.e., lift-to-drag ratio ( $L/D$ ), is actually improved at moderate and high angles of attack as the leading-edge flaps are deflected. The leading-edge flap has little effect on the pitching moment. On the other hand, with deflection of the trailing-edge flap, i.e. the S000010 and S301210 models, are significantly increased but the drag is larger than the S000000 and S301200 models that trailing-edge flap is not deflected, respectively. Because the trailing-edge flap has effect of increasing the wing camber and increase the suction force on the rear part of the wing, the pitching-down moment is increased. By combining the effects of the drag reduction due to the leading-edge flap and the lift increment due to the trailing-edge flap, the lift-to-drag of the S301210 model is improved by 46% at the lift  $CL=0.5\sim 0.6$ , which is close to the design condition of takeoff and landing situations.



(a) lift, drag, moment vs. angle of attack



(b) lift-drag polar

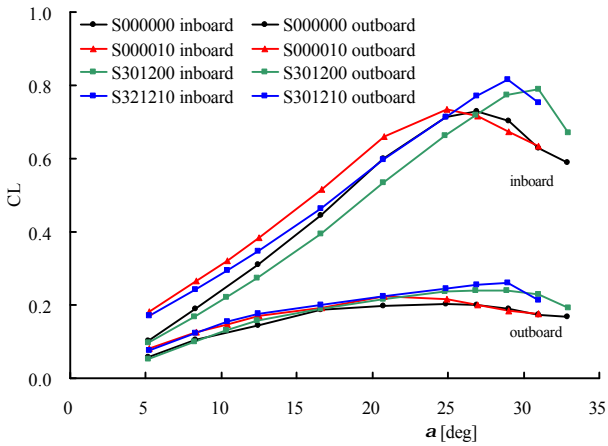
Fig. 4 Aerodynamic characteristics

Component lift and drag of the inboard and outboard wings, as shown in Fig. 5, are further calculated by using computational results. Due to the leading-edge vortex, the lift of the inboard wing is non-linearly increased with the angle of

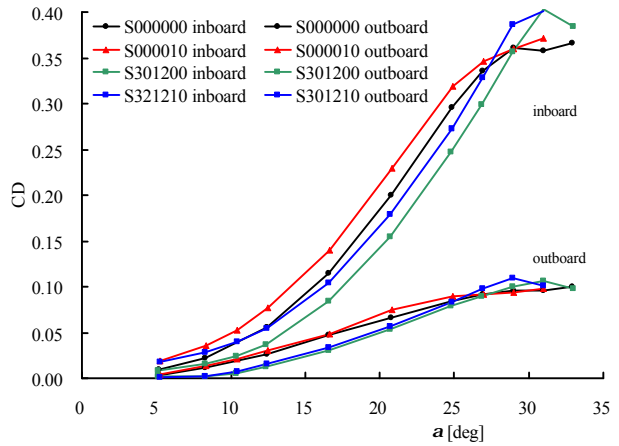
attack. In contrast, without the leading-edge flap, the outboard wings of the S000000 and S000010 models lose their lift increment early as the angle of attack is larger than  $10^\circ$ , and gradually approaches to stall at  $20^\circ$ . Because the

outboard wing has a small sweep angle and a sharp leading-edge, the stall is occurred much more early than that of the inboard wing. For the S301200 and S301210 models, the deflected leading-edge flap suppresses the leading-edge separation and has effect to delay the angle of attack when stall occurs. It is found that the total lift decrease due to deflection of the leading-edge flap is mostly contributed by the inboard

wing, while the lift of the outboard wing is slightly increased. On the other hand, drags of both the inboard and outboard wings are reduced by the leading-edge flap. The trailing-edge flap increase the drag of the inboard wing, but it has little effect on the drag of the outboard wing. It indicates that the leading-edge flap is more efficient on the outboard wing than the inboard wing at the condition of interest.



(a) lift

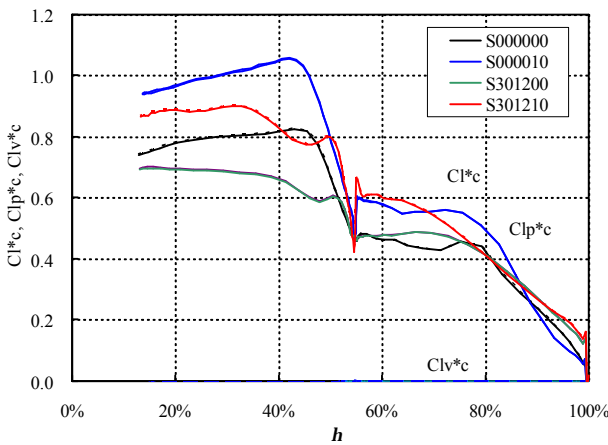


(b) drag

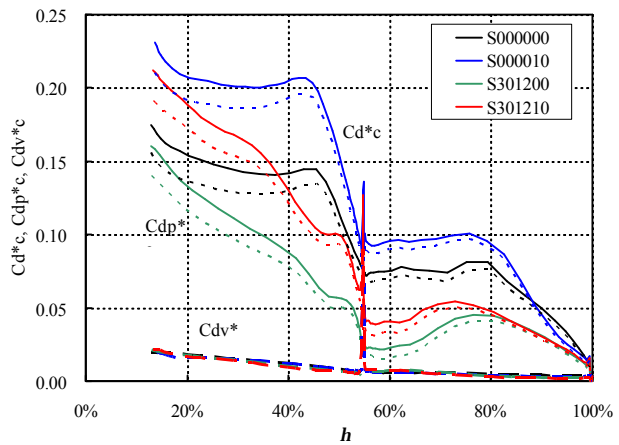
Fig. 5 Component contributions of aerodynamic forces.

Furthermore, spanwise load distributions are calculated and results of the AoA 12° are shown in Fig. 6. As the trailing-edge flap is deflected, both the lift and drag loads of the wing are increased. In contrast, the leading-edge flap is more effective on drag reduction than lift decrease. For the outboard wing, due to the delay of stall, the lift load is slightly changed, while the drag load is largely reduced. Compared with

the baseline S000000 model, the S301210 model, which combined the leading-edge and trailing-edge flaps, has larger lift load and small drag load. Another fact is that, even though there is large separation on the wing, the friction drag is dependent neither on the angle of attack nor on the deflection of the flap, but it is generally largely dependent on the surface area and the Reynolds number.



(a) lift



(b) drag

Fig. 6 spanwise load distributions at AoA=12°.

## 4.2 Surface Pressure

From surface pressure distributions of computation at  $AoA=12^\circ$  in Fig. 7, it is noted that as the leading-edge flap is deflected, the suction peak of pressure becomes weak and the low pressure region is significantly decreased on the upper surface of the inboard wing, thus this results in lift decrease. In contrast, on the upper surface of the outboard wing, although the suction peak

also becomes weak, the low pressure area is enlarged near the leading edge due to the delay of stall. So the total change in lift of the outboard wing is small. With deflection of the trailing-edge flap, the strong downwash influences the flow of not only the inboard but also outboard wings. The pressure of the upper surface of the trailing-edge flap and outboard wing becomes small. This results in increment of the lift.

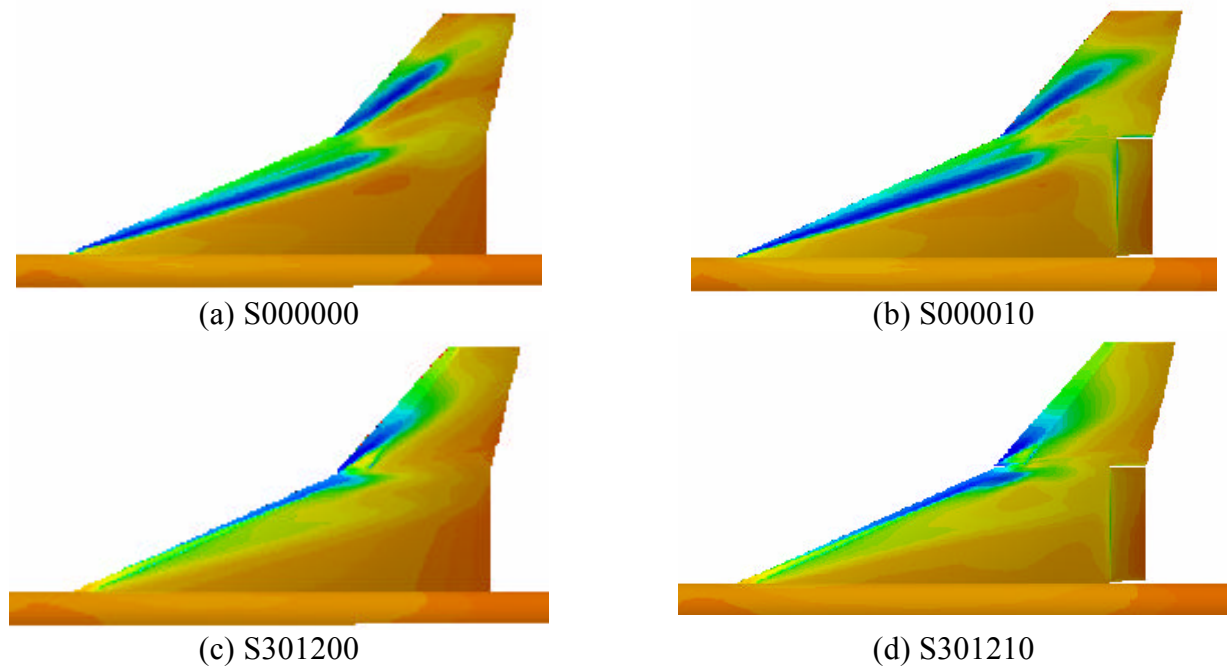


Fig. 7 Pressure distributions on the upper surface at  $AoA=12^\circ$ .

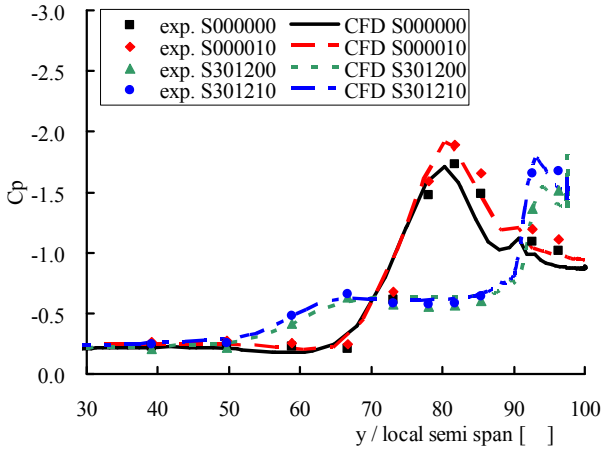
Pressure distributions at the two chordwise stations are compared with experiment in Fig. 8. The computation successfully captures the main features and is agreed well with experiment. Both primary and secondary vortices are well reproduced. However, the calculated locations of vortex breakdown are more upstream than that observed in the experiment. Suction peaks indicate the primary vortices separated from the leading edge. At the  $AoA 12^\circ$ , pressure suction of the inboard vortex is moved to the leading-edge and the radius of the vortex core becomes small, as shown in Fig. 8(a). The inboard vortex is burst at the upstream of the location  $X=0.83C_r$  in the computation, as shown in Fig. 8(b), and this results in a large difference of pressure near the vortex. The pressure suction

becomes larger due to downwash flow induced by the deflected trailing-edge flap.

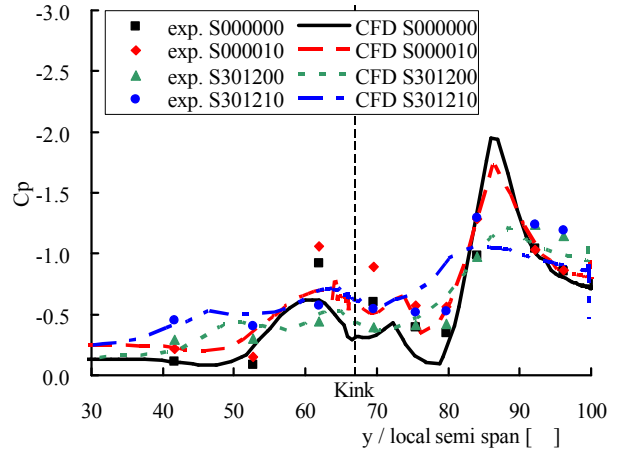
Distributions of pressure coefficient at several spanwise stations on the surface are extracted from the computational results, as shown in Fig. 9. In all cases, in the vicinity of the leading-edge, pressure is changed so rapidly that the strong adverse gradient results in a sudden separation. Distinct pressure suction peaks are found at the early stage of the vortex development, i.e.,  $h=0.3$  and  $0.6$  for the inboard and outboard wings, respectively. On the inboard wing, the pressure suction peak is moved to the leading-edge and the suction area becomes small. It indicates the section lift is decreased as the leading-edge flap is deflected. This results in a lift loss as mentioned above. By deflecting the trailing-edge flap, pressure is

decreased on the upper surface and increased on the lower surface of the trailing-edge flap.

This generated large increment of the lift and pitching-down moment.

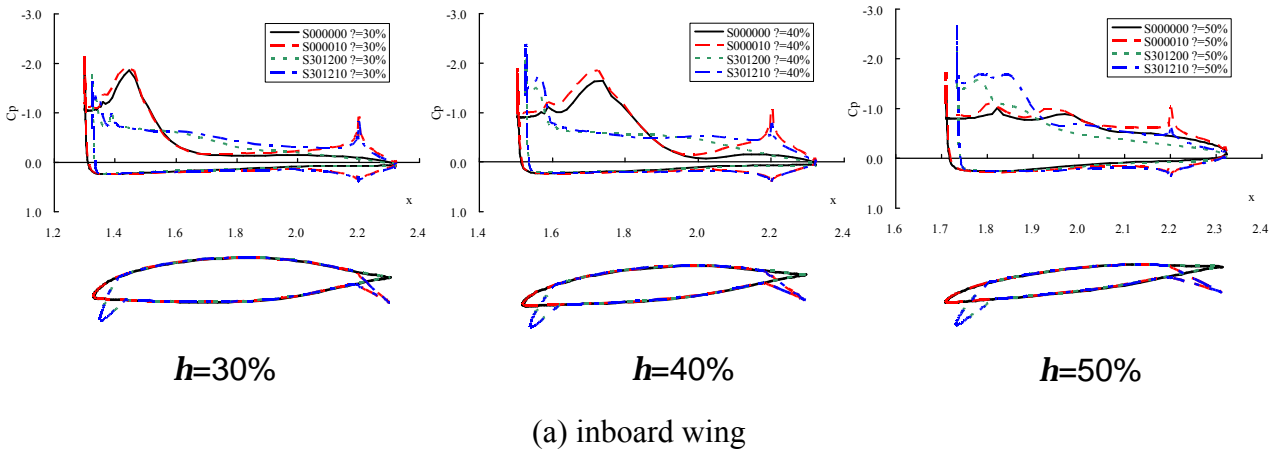


(a)  $X=0.55C_r$

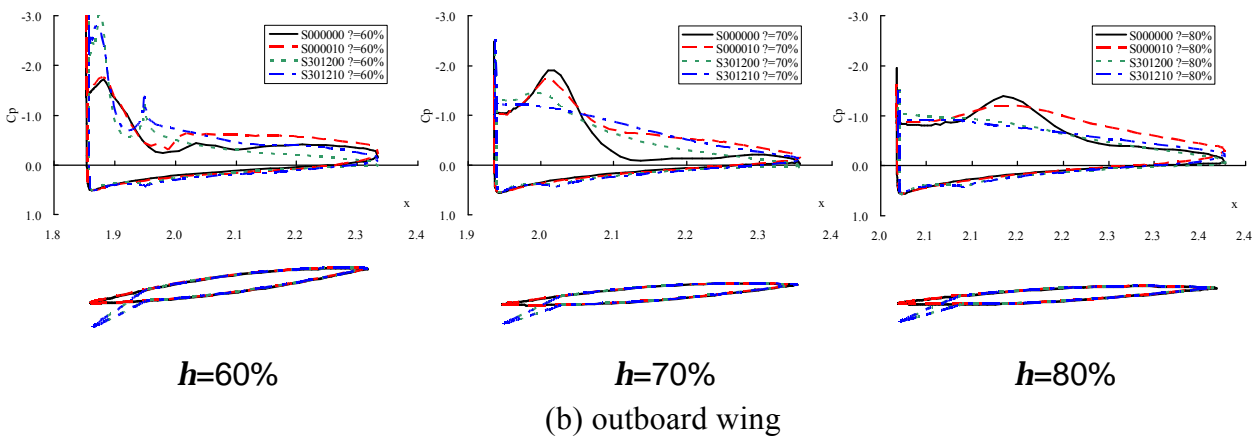


(b)  $X=0.83C_r$

Fig. 8 Pressure coefficients on the upper surface at  $AoA=12^\circ$ .



(a) inboard wing



(b) outboard wing

Fig. 9 Distributions of surface pressure coefficients at different spanwise stations at  $AoA=12^\circ$

### 4.3 Flow Structure

In Fig. 10, computed velocity distributions are given at the same chordwise stations  $X=0.55Cr$  and  $X=0.83Cr$  corresponding to Fig. 8. On the upper surface of the inboard wing, as the leading-edge flap is deflected, the leading-edge separation vortices move toward the leading edge and the wall, and reduced both in the size and in strength. The vortex cores becomes small and weak, and the vortex breakdown is delayed. At this deflection, the leading-edge vortex is restricted on the flap. It is also found that a vortex is generated near the surface from the hinge line of the flap. Although a hingeline separation is occurred at this situation, the size is very small and the vortex is very weak as compared with the leading edge one. The hingeline separation should not have large influence on the aerodynamic characteristics. At the station  $X=0.83Cr$ , with the trailing-edge flap, the size of the burst vortex becomes larger and this indicates vortex breakdown is occurred more upstream. The breakdown of the inboard vortex is prompted by the trailing-edge flap.

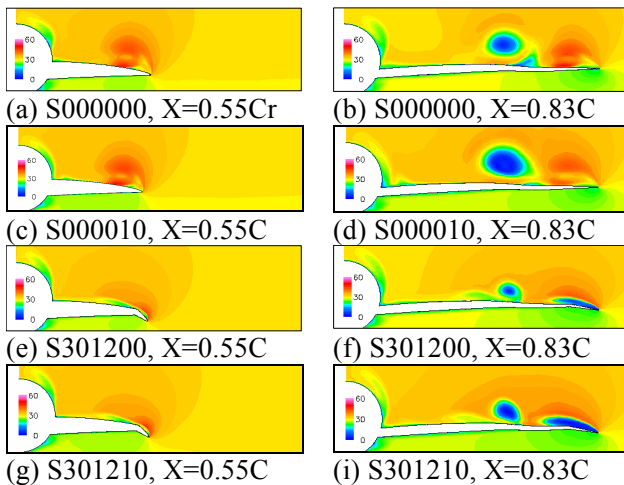


Fig. 10 Comparison of velocity magnitude at  $AoA=12^\circ$ .

Computed oil-flow patterns on the wing upper surface are given in Fig. 11. Converged lines represent separation and diverged ones

represent reattachment. The primary and secondary vortices can be clearly identified by the limiting streamlines on the surface. The inner vortices are originated from the intersection point of the wing leading edge and the body. And the outer vortices are originated from the kink of the inboard and outboard wing. Both inner and outer vortices are separated from the leading edge. For the S000000 and S000010 models, large separation regions are confirmed on the wing upper surface. By deflecting the leading-edge flap, like the S301200 and S301210 models, makes the separation vortices reattach on the surface of the leading-edge flap. A large attached region of flow is observed on the wing surface. The inboard leading-edge vortex is completely located on the flap, and bent to the direction of the free-stream at the leading edge kink. Most part of the outboard leading edge vortex is moved to the flap. The stream-wise length becomes short and the separation region is very small. Instead, the attached region of flow is enlarged. Both leading-edge vortices of the inboard and outboard wing are located on the flap upper surface, and a typical vortex flap is achieved as this flap deflection.

In the present cases, viscous effect in the boundary layer and separation vortex is the only factor that makes the total pressure lose. In Fig. 12, distributions of total pressure loss are provided at several spanwise stations. It can be seen that both the inboard and outboard leading-edge vortices are continuously fed with vorticity by separated shear layer from the leading edge, bent at the kink and wing tip, and eventually convects longitudinally downstream. The large the separation, the more the total pressure is lost. As the leading-edge flaps are deflected, the level of total pressure loss is reduced, and the total pressure is less lost. As a result, the drag is reduced. Conversely, the trailing-edge flap makes the vortex large in strength and size, thus the drag is increased. The combination of leading-edge and trailing-edge flap has smallest total pressure loss, and it is the most efficient.

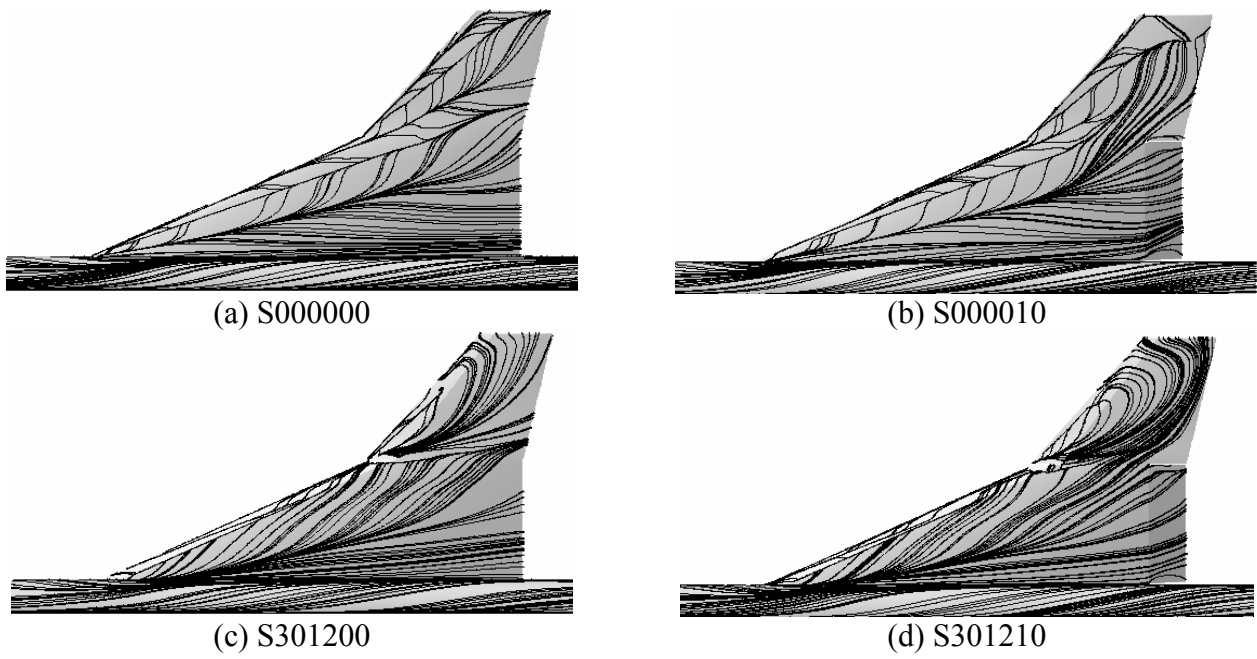


Fig. 11 Computed oil-flow pattern on the upper surface at AoA=12°.

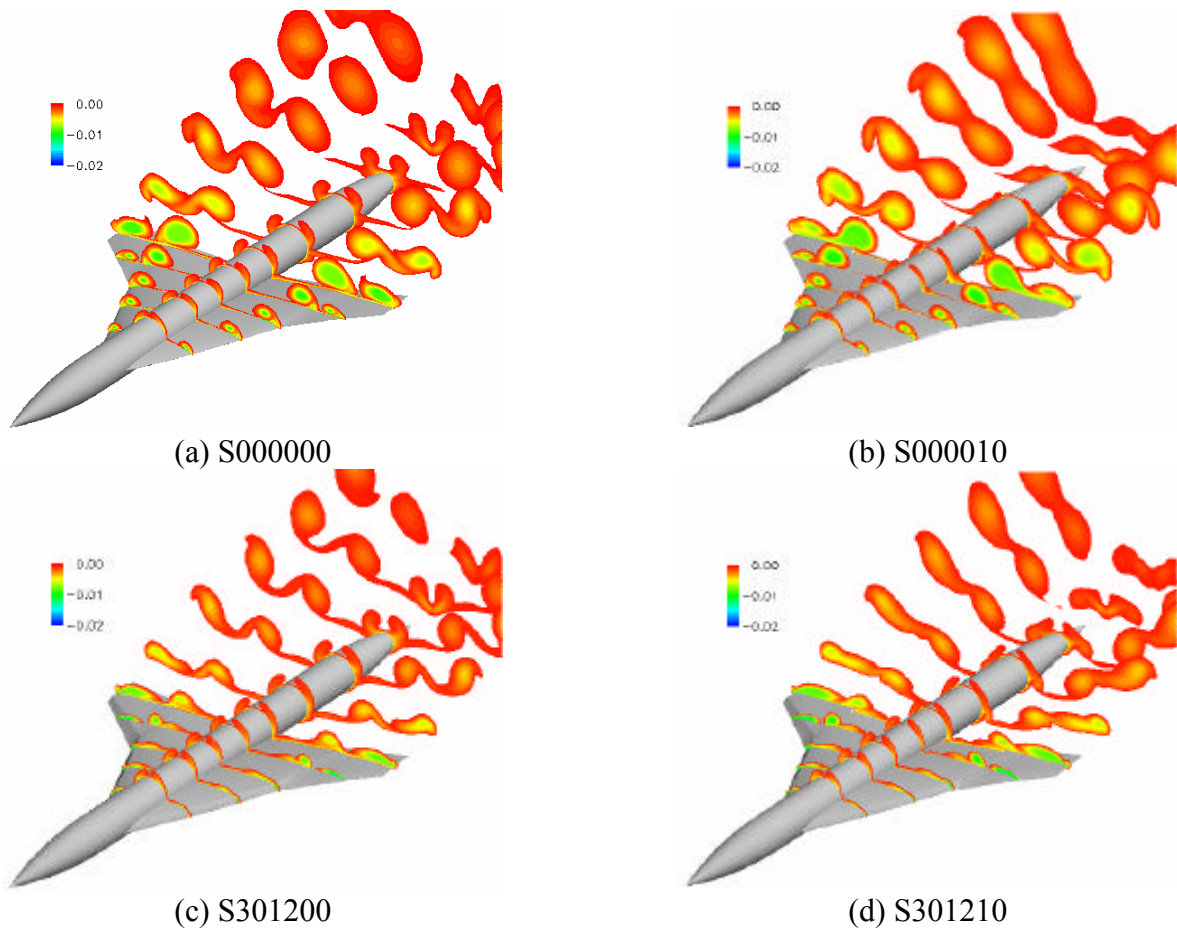


Fig. 12 Computed total pressure loss at AoA=12°.

## 5 Conclusions

Flow around a supersonic transport configuration with high-lift devices is investigated at low speed conditions by experiment and numerical simulation. The leading-edge and trailing-edge flaps have effect of improving the aerodynamic performance from the baseline configuration. Wind tunnel test is conducted to obtain aerodynamic characteristics. The Reynolds-averaged Navier-Stokes equations are solved, and the computational results are used to analyze the details of the flow field. Major conclusions are summarized as follows.

1. As the leading-edge flap is deflected, both lift and drag of the inboard wing is decreased, while for the outboard wing, the lift is enhanced and the drag is reduced due to the delay of the stall. With increase of the flap deflection, the leading-edge vortex is reduced both in size and in strength. At a large deflection, the leading edge vortices are located on the flap upper side, and a typical vortex flap is confirmed.

2. The trailing-edge flap increases effective camber of the wing, and pressure is decreased on the upper surface and increased on the lower surface of the trailing-edge flap. It generates large increment of the lift and pitching-down moment.

3. Combination of the leading-edge and trailing-edge flaps has advantage to increase the lift, and reduce the drag at the same time. It largely improves the lift-to-drag ratio by 46% at the lift  $CL=0.5\sim 0.6$ .

4. Validation shows that the numerical simulation provides an accurate prediction of aerodynamic characteristics and captures flow features reasonably well as compared with experiment.

## References

- [1] Antani, D.L. and Morgenstern, J.M. HSCT High-Lift Aerodynamic Technology Requirements. *AIAA paper* 92-4228.
- [2] 1998 NASA High Speed Research Program Aerodynamic Performance Workshop. *NASA CP-1999-209682*.
- [3] Herrmann, U. Low-Speed High-Lift Performance Improvements Obtained and Validated by the EC-Project EPISTLE, *24th International Congress of the Aeronautical Sciences*, ICASE-2004-411, August 29 – September 3, Yokohama, Japan.
- [4] Rao, D.M. Exploratory Subsonic Investigation of Vortex Flap Concept on Arrow-Wing Configuration. *Supersonic Cruise Research '79*, Part I, NASA CP-2108, 1980.
- [5] Yoshida K and Makino Y. Aerodynamic design of unmanned and scaled experimental airplane in Japan. *ECCOMAS 2004*, Jyväskylä.
- [6] Kwak, D., Miyata, K., Noguchi, M., Sunada, Y. and Rinoie, K. Experimental Investigation of High Lift Device for SST. *NAL TR-1450*, National Aerospace Laboratory, 2002.
- [7] Lei, Z. Effect of RANS Turbulence Models on Computations of Separated Flows over a Wing-Body Configuration. *Transaction of JSASS*, Vol.48, No.161., 2005.